



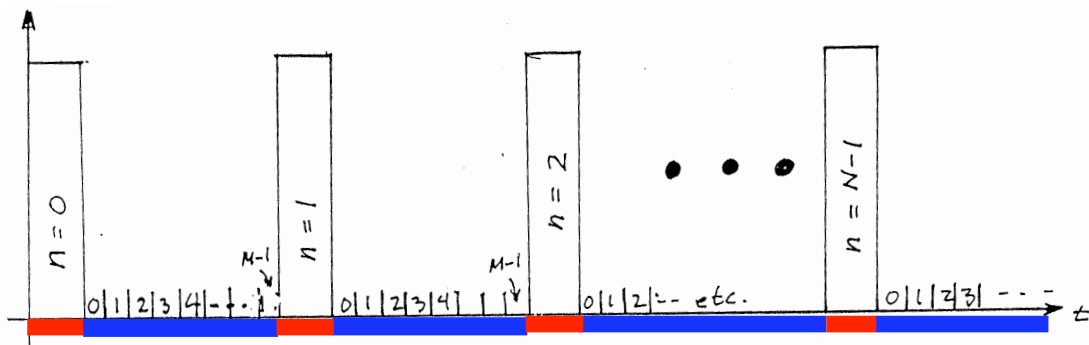
*Session 32*

**The Pulse Waveform  
Delay-Doppler Processor**

## Recall...

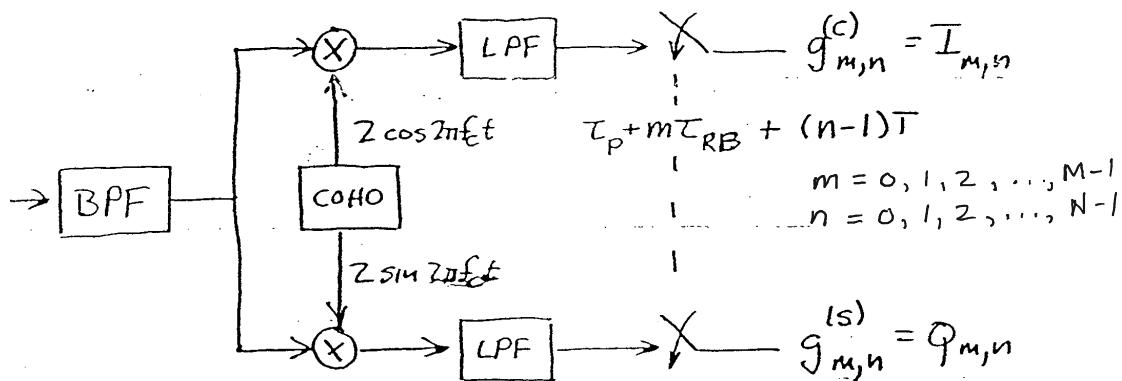
So we will divide the listening period into time bins of width  $T_{RB}$  and sample the signal once per bin for each range bin of interest.

Label the range bins  $0, 1, \dots, M-1$ .



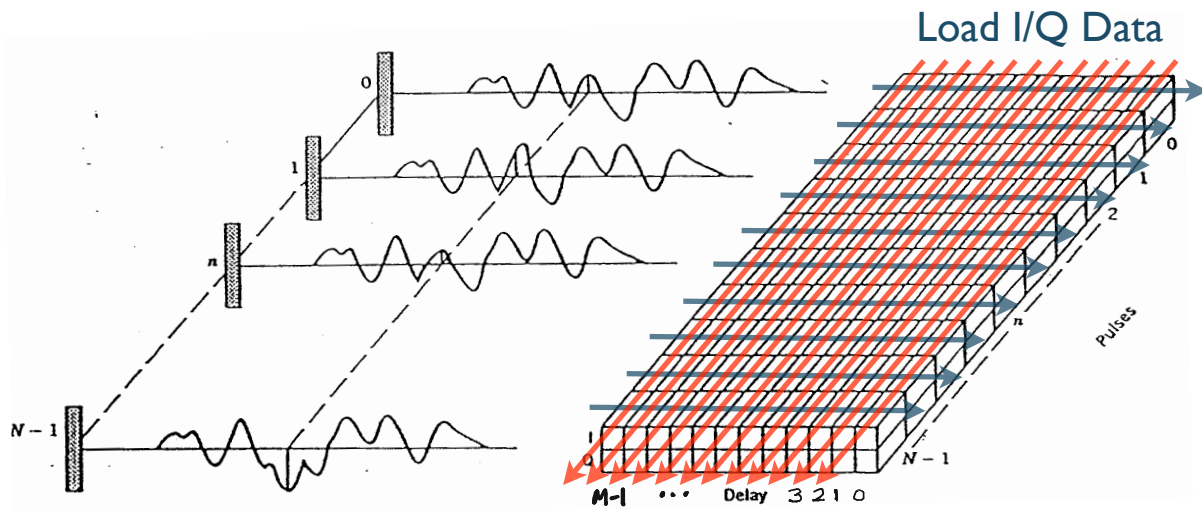
## Recall...

We can get the sample returns from each of the range bins (both I and Q components to represent the complex baseband signal) by processing the received signal as follows:



n.b.,  $\tau_p$  is the transmitted pulse duration.

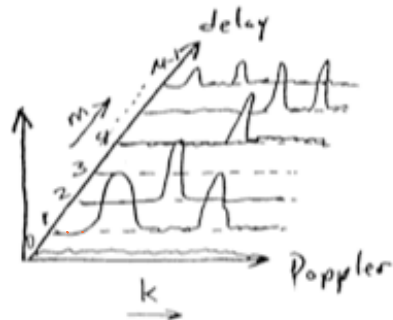
Recall...



Compute DFT for each range cell

Recall...

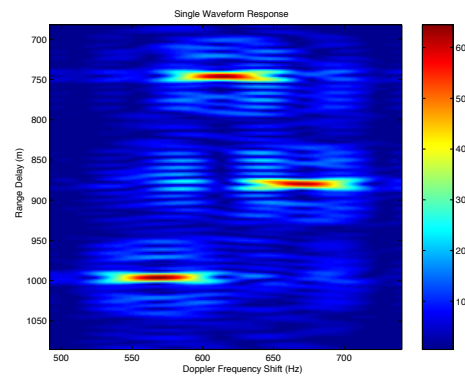
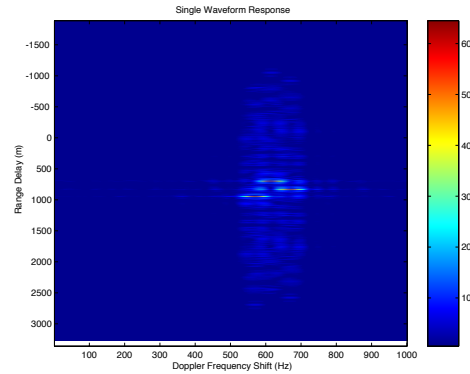
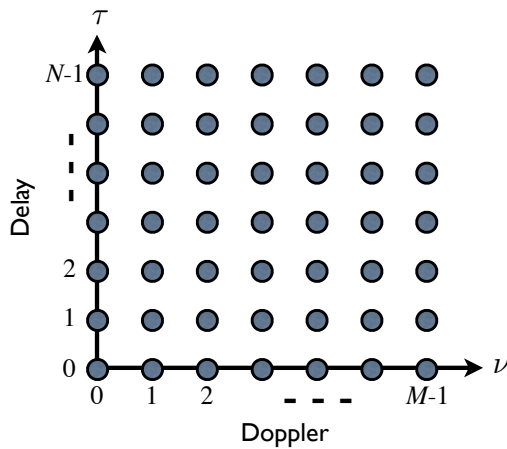
If we process in this way for each range cell (each  $m$ ), we can construct a "Delay-Doppler" spectrum



From such a Delay-Doppler image one can detect where the targets are in Delay and Doppler ( $\tau$  and  $\nu$ ).

## Recall...

Actually, because delay range bins are discrete and the Doppler response is computed using a DFT, we get a discrete map of delay-Doppler space:



## Recall...

Of course the DFT response  $G_k$  will be maximum for a target Doppler  $f_D$  such that

$$f_D = \frac{k}{NT} + m \cdot \frac{1}{T}$$

however, for other  $f_D \approx \frac{k}{NT}$ , DFT response will also be large.

n.b  $G_k \equiv 0 \Leftrightarrow f_D = \frac{j}{NT}, j \neq k.$

It can be shown that the normalized response of the  $k$ -th Doppler filter  $G_k$  to a target with Doppler frequency  $f_D$  is

$$|\hat{G}_k(f_D)| = \frac{1}{N} \left| \frac{\sin[\pi N(f_D T - k/N)]}{\sin[\pi(f_D T - k/N)]} \right|$$

$$|\hat{G}_k(f_D)| = \frac{1}{N} \left| \frac{\sin[\pi N(f_D T - k/N)]}{\sin[\pi(f_D T - k/N)]} \right|$$

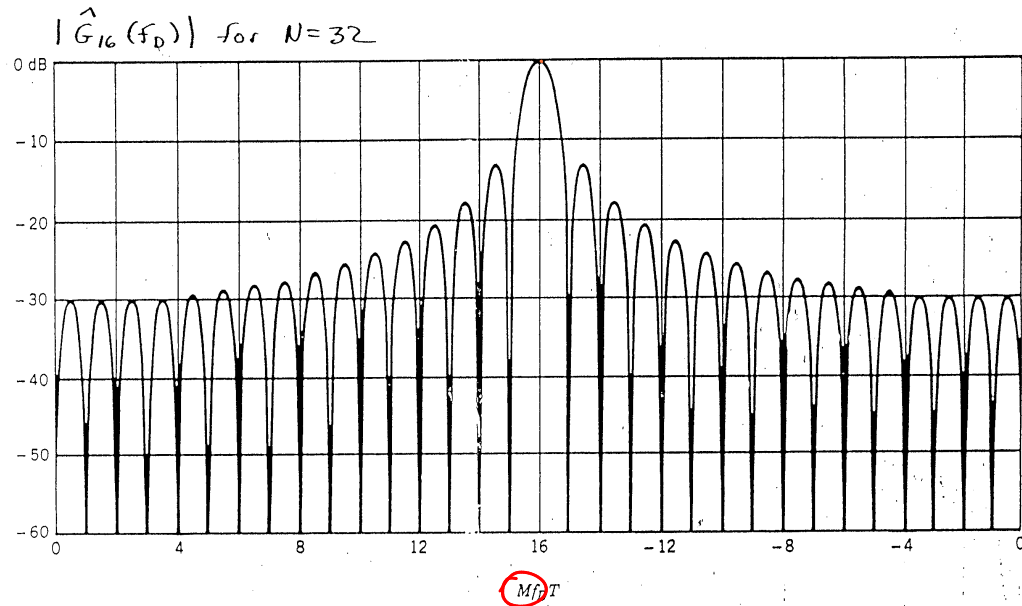


Figure 10.6 Frequency response of the 16th filter in an  $N = M = 32$  DFT with a rectangular weighting.

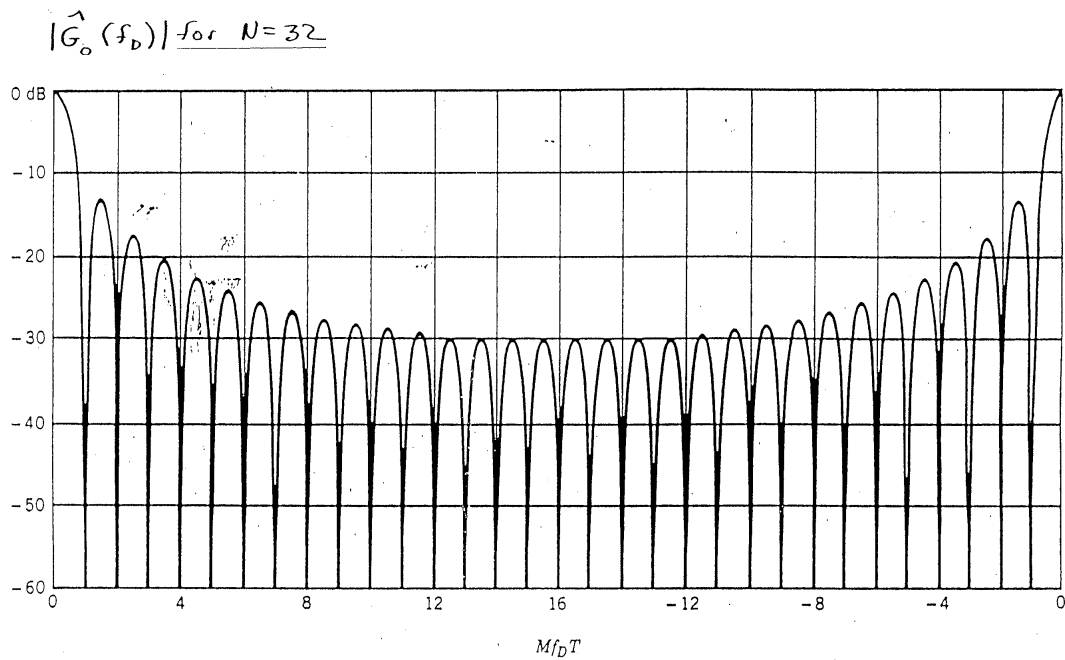


Figure 10.5 Frequency response of the zeroth filter in an  $N = M = 32$  DFT with a rectangular weighting.

Sidelobes can be reduced with windowing  
before taking the DFT

$$\sum_{n=0}^{N-1} u_n \cdot w_n e^{-i \frac{2\pi n k}{N}}$$

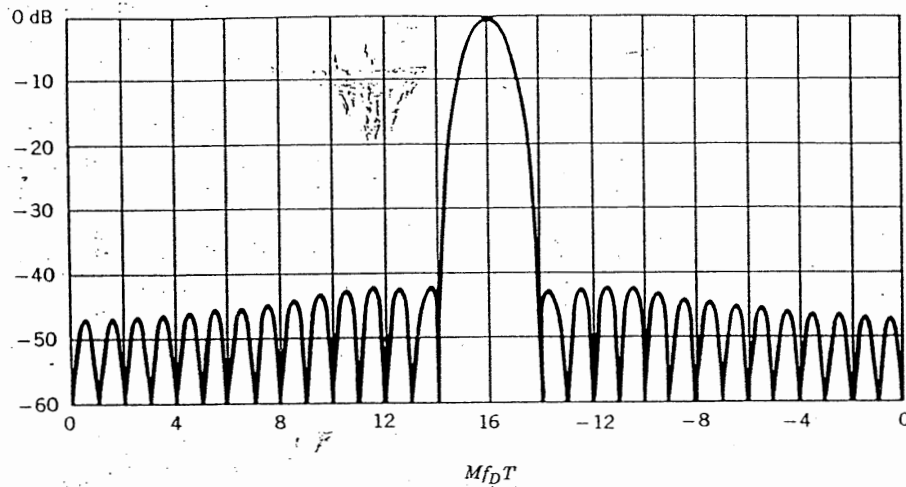


Figure 10.7 Frequency response of an  $N = M = 32$  DFT, Hamming weighting.

Hamming Window:  $w_n = a_0 - a_1 \cos\left(\frac{2\pi n}{N}\right)$   
 $a_0 = 0.53836$   
 $a_1 = 0.46164$

Sidelobes can be reduced with windowing  
before taking the DFT

Hann (Julius Von Hann) Window: Same as Hamming, but  
 $a_0 = a_1 = 1/2$ .

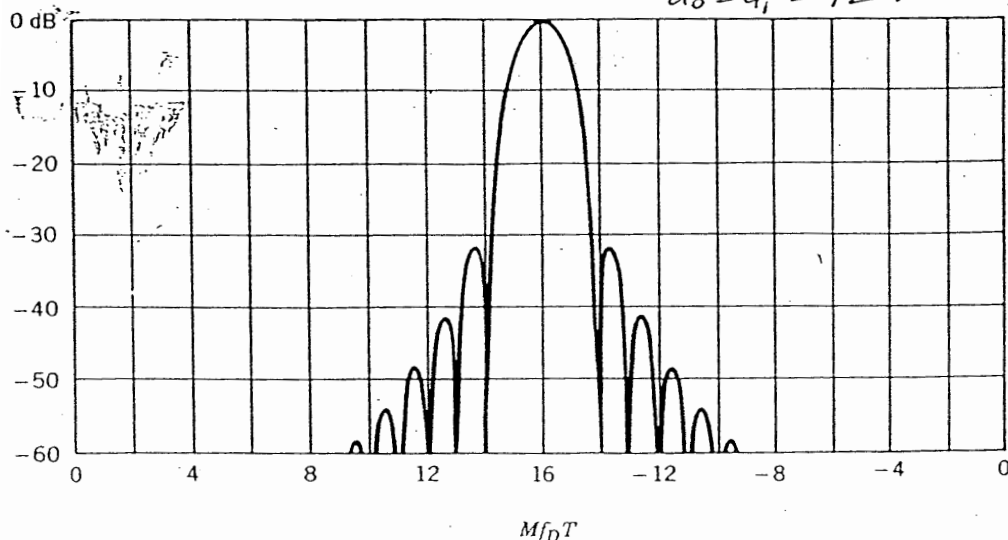


Figure 10.8 Frequency response of an  $N = M = 32$  DFT, Hann weighting.

# Comparison of Windows

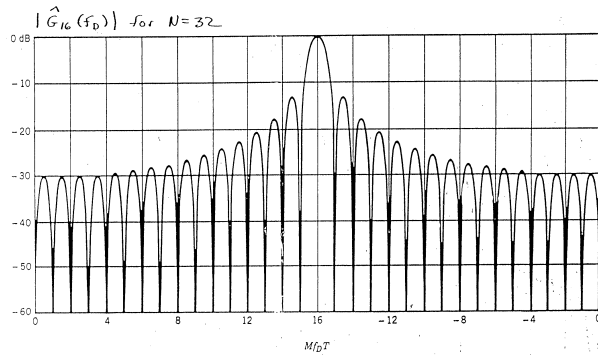


Figure 10.6 Frequency response of the 16th filter in an  $N = M = 32$  DFT with a rectangular weighting.

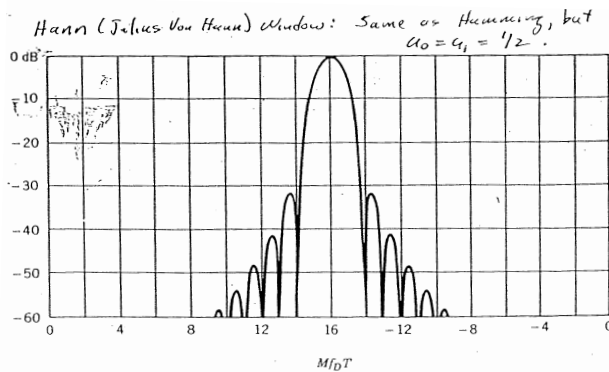


Figure 10.8 Frequency response of an  $N = M = 32$  DFT, Hann weighting.

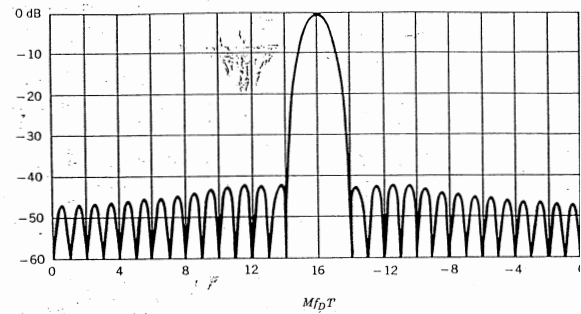
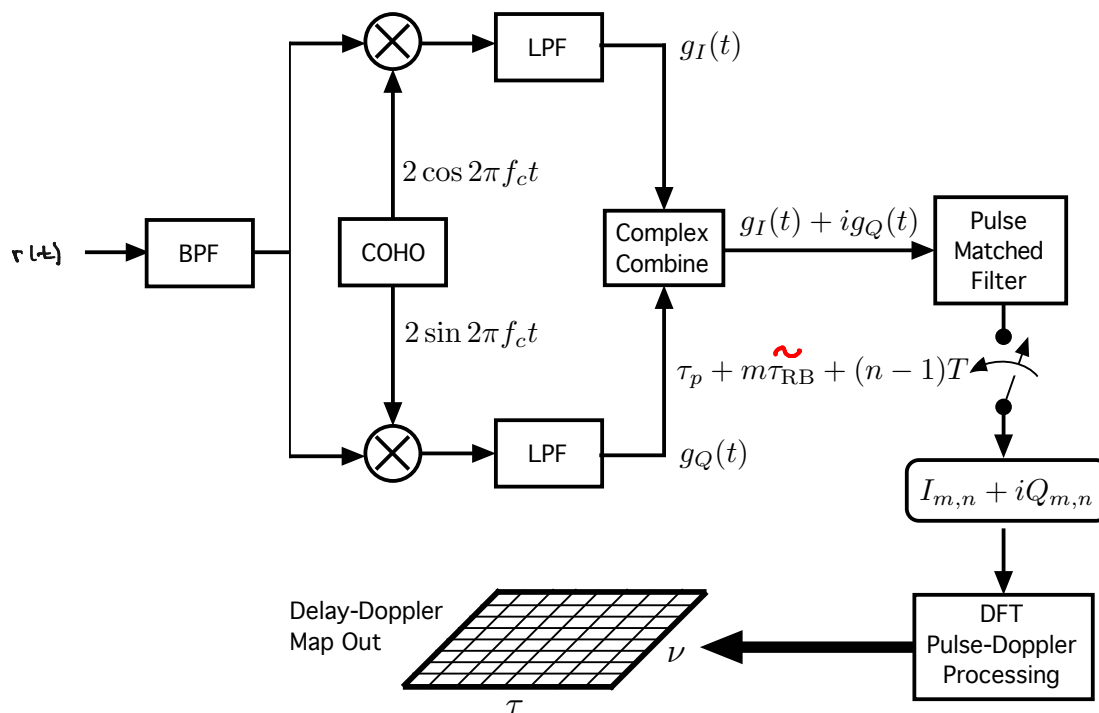


Figure 10.7 Frequency response of an  $N = M = 32$  DFT, Hamming weighting.

Hamming Window:  $w_n = a_0 - a_1 \cos\left(\frac{2\pi n}{N}\right)$   
 $a_0 = 0.53836$   
 $a_1 = 0.46164$

# Including the Matched Filter



# Coded Radar Signals

Reference: N. Levanon and E. Mozeson, *Radar Signals*, Wiley, 2004 (ISBN 0-471-47378-2)

- We will consider coded radar “pulses” as opposed to pulse trains.
- We have already seen that modulation of a radar pulse (e.g. a “chirp”) increases the range resolution of the signal through bandwidth expansion.
- Modulation of a radar pulse can significantly modify its ambiguity function (e.g. the “sheared” ambiguity function generated by a chirp)
- We want to consider intelligent approaches to modulating waveforms
- Coded waveforms provide a structured approach to designing waveforms.